Fiber optic probe hydrophone for the study of acoustic cavitation in water

Arnaud Arvengas, Kristina Davitt, and Frédéric Caupin[a)]
Laboratoire de Physique Statistique, Ecole Normale Supérieure, UPMC Université Paris 06, Université Paris Diderot, CNRS, 24 rue Lhomond, 75005 Paris, France

(Received 25 November 2010; accepted 31 January 2011; published online 15 March 2011)

We use focused ultrasound bursts to submit a liquid to mechanical tension. When the pressure in the sound wave reaches a sufficiently low value, vapor bubbles are nucleated in the bulk liquid. According to nucleation theory, increasing the ultrasound frequency increases the cavitation threshold by a calculable amount. To check this, we have built a fiber optic probe hydrophone based on one originally proposed by Staudenraus and Eisenmenger [Ultrasonics **31**, 267 (1993)]. We have adapted the pressure calibration and data analysis of this tool to make it appropriate for precise measurements of tension in liquids. We are able to resolve the fractional change in the pressure threshold for cavitation in water that results from a twofold increase in the frequency. This provides a test of nucleation theory in general. © *2011 American Institute of Physics*. [doi:10.1063/1.3557420]

I. INTRODUCTION

Owing to cohesion forces, a liquid can sustain mechanical tension, in which case the pressure may reach negative values.[1,2] We use an acoustic wave to stretch liquids to negative pressure, until they break by nucleation of a vapor bubble in a process called cavitation.[3] To make a quantitative comparison of the cavitation threshold between theory and experiment, an accurate measurement of the pressure in the wave is required.

The measurement of sound wave amplitudes has been addressed by a number of methods[4] and is crucial for medical applications that use high power ultrasound.[5,6] In 1993, Staudenraus and Eisenmenger[7] first introduced the fiber optic probe hydrophone (FOPH), a tool that uses the reflection of light at the fiber–liquid interface to measure the amplitude of a sound wave. The fiber is made of silica, which is completely wet by most liquids, and therefore does not increase the cavitation probability. Cavitation events can damage a probe; however, the fiber hydrophone is easily recleaved. For these reasons, the FOPH is an ideal tool to study acoustic cavitation.

We have built a FOPH and adapted the pressure calibration and data analysis with special attention to the case of liquids under tension. In particular, we advocate the use of physically appropriate equations to ensure a reliable conversion of the raw signal into pressure in the acoustic wave even for negative pressures. Effort has been made to quantify both uncertainties due to measurement noise and systematic uncertainties introduced by assumptions in the analysis procedure. This has allowed us to turn the FOPH into an instrument of sufficient accuracy to study the details of the physical process of cavitation.

The value of an accurate hydrophone is illustrated with results on cavitation in water. Liquid water represents an extreme case of cohesion, as illustrated by its high surface tension—which is one of the macroscopic manifestations of water's hydrogen bond network. Water exhibits numerous anomalies, for which several contending explanations have been proposed.[8–10] Knowledge of the cavitation threshold of water may provide insight into this ongoing debate.[11] However, cavitation experiments in water have found conflicting results.[12,13] Thus, a test of nucleation theory applied to water is of particular interest as it may establish whether the measured threshold corresponds to a nucleation process or is an artifact of the measurement method. Here, we report on an experiment to test the kinetic aspect of nucleation theory. By increasing the frequency of the sound wave, we reduce the effective volume and duration of the applied tension. Under these conditions, nucleation theory predicts an increase in the cavitation threshold. The FOPH is able to measure this change and direct comparison with the theory, without any adjustable parameters, shows a good agreement.

II. EXPERIMENTAL SETUP

Here we briefly describe the apparatus used to generate acoustic bursts and the hardware used to implement the FOPH before carefully describing the specific changes made to the calibration and data analysis procedures.

A. Acoustic setup

The piezoelectric transducers used to generate acoustic waves are similar to those used in our previous studies:[3,13] hemispherical shells of ceramic material C5800 (Channel Industries, California). In this paper, two different shells are used. Both are excited at their thickness mode resonant frequency, which is either 1 or 2 MHz. The transducer, which is varnished to reduce oxidation of the electrodes, is immersed in ultrapure water produced by a commercial purification system (Direct-Q, Millipore) and placed in a Pyrex container open to the air. We have checked that these conditions do not affect the cavitation results by comparing to experiments performed with degassed water which was transferred under vacuum to a dedicated cell.[3,14] The advantage of the present setup is that it allows easy access to the acoustic focal point.

[a)]Present address: Laboratoire de Physique de la Matière Condensée et Nanostructures, Université Claude Bernard Lyon 1 et CNRS, Institut Universitaire de France, 43 boulevard du 11 novembre 1918, 69622 Villeurbanne Cedex, France. Electronic mail: frederic.caupin@univ-lyon1.fr.

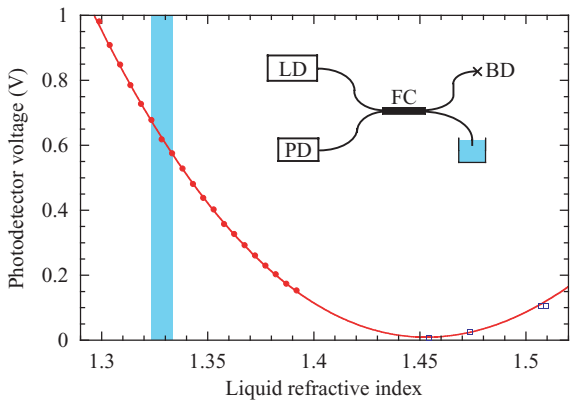

FIG. 1. (Color online) PD voltage as a function of liquid index. The data (filled red circles) are fitted with Eq. (2) (red curve). The error bars are smaller than the symbol size. Additional data points (open blue squares) confirm the quality of the fit. The range of interest for our acoustic measurements in water is indicated by the shaded area. Inset shows a sketch of the FOPH apparatus.

B. Fiber optic probe hydrophone

The general FOPH setup, illustrated in the inset of Fig. 1, has been described previously (Refs. 7 and 15). Here we provide technical details of our implementation. We use a pigtailed laser diode module (LD, High Power Devices), with a maximum power of 400 mW at 808 nm. It is driven by a standard laser power supply (Thorlabs LDC220) and is temperature-stabilized by an external controller (Thorlabs TED350). The LD, which is operated in constant power mode, is connected to one input of a 2×2 fiber coupler (FC) with a nominally 3 dB splitting ratio. The fiber coupler constitutes the main part of the apparatus. It was custom fabricated by fusion splicing (AFW Technologies) from a multimode, pure silica step-index fiber (Thorlabs AFS50/125Y) with core/cladding diameters of $50/125\ \mu$m. The end facet of one output is cleaved at an angle of 8° and connected to a beam dump (BD, Newport −70dB). We find that this method of reducing the reflection from this unused arm is more efficient than leaving it immersed in distilled water, as proposed in Ref. 15. The other output of the coupler constitutes the measuring arm. When it is immersed in a fluid, because of the refractive index mismatch with pure silica, a small fraction of the laser light is reflected and propagates back into the coupler, approximately half reaching a photodetector (TIA-525, Terahertz Technologies) at the second input of the coupler. The photodetector (PD) consists of a silicon photodiode and amplifier with a first stage 1.4 kΩ transimpedance and a second stage gain of 10. This combination has a high frequency cutoff at 135 MHz, and the linearity of photoresponse has been verified up to 3.5 mW at 633 nm (a power larger than any encountered in the experiments described here) by comparing to a calibrated large area detector.

C. Fiber preparation and positioning

The quality of the measurement depends critically on the preparation of the end facet of the measuring arm. After removing its coating, the fiber is cleaved perpendicularly to its axis using an ultrasonic fiber cleaver (Photon Kinetics FK11). The condition of the facet can be monitored at any time by a standard measurement (see Sec. III B). When it is damaged, the FOPH can be easily regenerated by recleaving.

In some fiber hydrophone implementations, the end facet is modified with one or more layers of other reflective materials to create a miniature Fabry–Perot interferometer[16–18] and thereby increase the sensitivity. Tapered fibers have also been used to increase the FOPH bandwidth;[19] their sensitivity can also be increased by the addition of a thin gold layer.[20] In this work, we chose to keep the bare fused silica tip, without further treatment after cleaving, which makes regeneration easier and allows a straightforward calibration (Sec. III).

Easy positioning of the measuring arm is required in order to explore the acoustic field. The fiber is held in position with a clamp located approximately 5 mm from the exposed area on the loose tube jacket. The length of hanging fiber is deliberately kept short to prevent displacement by the ultrasonic wave. Here we use the FOPH in a sound beam with the end facet normal to the beam axis. However, we have checked that the measurement does not depend on the fiber orientation, as expected.[15]

III. CALIBRATION AND DATA ANALYSIS

In this section we describe the principle of measurement and how we have improved the calibration of the FOPH. We also propose a refined data analysis to deduce physical quantities from the measured electrical signal.

A. Principle of measurement

The FOPH relies on the reflectivity R of the interface between two media of different indices, which follows the Fresnel relation at normal incidence,

$$R = \left(\frac{n_f - n_l}{n_f + n_l}\right)^2, \tag{1}$$

where n_f and n_l are the fiber and liquid refractive indices, respectively.

Practically, the measured quantity is the voltage output of the PD amplifier,

$$V = G\,\frac{I_0}{4}(R + S), \tag{2}$$

where G is the PD responsivity, I_0 the intensity at the output of the LD, and the factor 4 accounts for the two passes through the nominally 3 dB coupler. The term S has been added to account for any stray light, which may arise from defects in the coupler (e.g., crosstalk between the two inputs) and/or from the unused output arm.

When a sound wave is present at the fiber–liquid interface, n_l and R are modulated in time,

$$n_l(t) = n_l^0 + \delta n_l(t) \quad \text{and} \quad R(t) = R_0 + S + \delta R(t), \tag{3}$$

where n_l^0 is the refractive index of the static liquid in the absence of any sound wave and R_0 is the corresponding static reflectivity. Together, the average dc-component just before the

wave reaches the FOPH (V_{dc}) and the ac-component [$V_{ac}(t)$] yield the modulation of the reflection coefficient,

$$\delta R(t) = \frac{V_{ac}(t)}{V_{dc}}(R_0 + S). \quad (4)$$

The interest of this procedure is that the values of G and I_0 are not needed. Finally, using Eq. (1), we obtain the index of the liquid,

$$\frac{n_1(t)}{n_f} = \frac{n_1^0 + \delta n_1(t)}{n_f} = \frac{1 - \sqrt{R_0 + \delta R(t)}}{1 + \sqrt{R_0 + \delta R(t)}}. \quad (5)$$

Typically, for water at 20 °C and 0.1 MPa, $n_1 = 1.3285$. Since $n_f = 1.453$ (see Sec. III B), $R_0 = 0.2\%$ and only 0.1 mW reaches the PD. The maximum modulation observed for our acoustic setup is 10%.

In practice, the PD signal is mixed with noise. When working with repetitive signals from many bursts, averaging may be used to reduce the noise; for our studies, an average over 100 bursts gives satisfactory results. We note that this may be improved by an elaborate treatment of the signal to remove the noise arising from intensity fluctuations of the LD, as is implemented in the original version of the FOPH.[7]

B. Calibration by reflectivity measurements

As can be seen from Eqs. (4) and (5), to determine the refractive index of the liquid, the parameter S must be known. It was originally proposed that S be "determined under zero reflectivity conditions—for instance, by immersing the fiber endface into an index-adapted fluid."[7,21] However, this provides only one data point to deduce S and one which falls well outside the range where the FOPH is used since usual liquids have a lower index than fused silica [1.453 at 808 nm (Ref. 22)]. Instead, as a thorough calibration of the entire system, we measure the dc PD voltage with the fiber sequentially immersed in a series of 20 calibrated microscope immersion liquids (Cargille AAA-series) to map the reflected light as a function of index around the index of water. These liquids are perfluorocarbon- and chlorofluorocarbon-based, and in order to clean the fiber between different liquids, the bare tip is placed in acetone. The dc reflection in acetone is also recorded to provide an estimate of the uncertainty in the reflected light power (±0.4 %) over the duration of the experiment.

Figure 1 shows the measured PD voltages, fitted with Eq. (2), with S and GI_0 treated as adjustable parameters. The fiber index was kept constant ($n_f = 1.453$). The procedure yields $S = (3 \pm 0.8) \times 10^{-5}$. The fit is very good, with a reduced $\chi^2 = 0.2$ likely indicative of an overestimation of the uncertainty in the index given by the manufacturer (0.00076). Assuming that all of the stray light can be attributed to the coupler alone, we find a very good directivity, better than −50 dB. Shown in Fig. 2, but not included in the fit, are four additional data points obtained using other immersion oils (Cargille, Types DF and FF, fused silica matching liquid 50350, and custom liquid 5095) that have indices greater than those of fused silica and thus allow us to visualize the minimum in the fit function. From the excellent match of this data to the fit curve, we can additionally conclude that the chosen index of fused silica is appropriate and that the detector and amplifier combination exhibits a linear photoresponse over the entire index range.

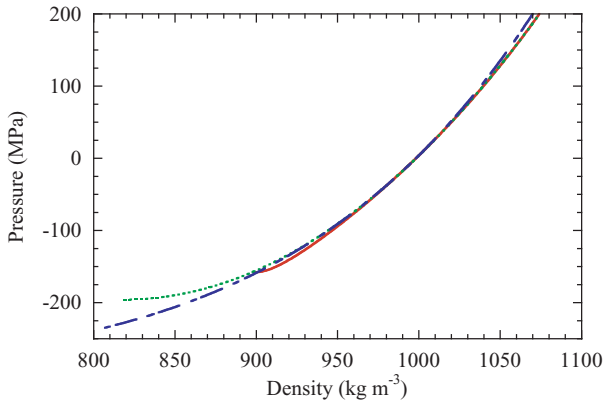

FIG. 2. (Color online) Comparison of several EoSs for water in the pressure-density plane and their extrapolations in the negative pressure region: isentropic Tait (dashed-dotted blue line), and isotherms from IAPWS-95 (solid red line) and Speedy (dotted green line). The two last EoSs stop at the spinodal limit with a horizontal tangent.

To monitor the quality of the FOPH, we follow the procedure recommended by Refs. 7 and 21. Prior to performing a series of FOPH measurements, the dc PD voltage is measured with the fiber in air and then immersed in water. The ratio β provides a quick check of the facet condition. Practically, we recleaved if β was larger than 0.065.

C. Conversion from refractive index into density

The FOPH directly measures the modulation of the refractive index of the liquid by the sound wave. To convert it into liquid density, Ref. 7 used the empirical Gladstone–Dale relation,

$$\rho = \rho_0 \frac{n_1 - 1}{n_1^0 - 1}, \quad (6)$$

which fits positive pressure data well "at dynamic compressions up to approximately 500 MPa, confirming the results obtained from static compression within an error limit of 5%." For the negative pressures ($\rho < \rho_0$) investigated in the present work, an extrapolation down to −30 MPa is required. To warrant the use of data obtained by extrapolation, we prefer to use a relation between n_1 and ρ that is based on a physical law. Following the International Association for the Properties of Water and Steam (IAPWS),[23] we use a modified version of the Lorentz–Lorenz[24] relation; see Appendix A for details. For the pressures obtained here, it agrees with the Gladstone–Dale relation to within 0.1%. Typically, for water at 20 °C and 0.1 MPa, a change of 0.3% in n corresponds to a change of around 1% in ρ.

D. Conversion from density into pressure

To determine a pressure from the density calculated above, one must rely on an equation of state (EoS). It is important to keep in mind that for water, use of an EoS at negative pressure constitutes an extrapolation for which little

supporting data exist. In the original work,[7] the isentropic Tait equation was used,

$$P = (P_0 + P_1)\left(\frac{\rho}{\rho_0}\right)^{\gamma} - P_1\,, \tag{7}$$

with $P_0 = 0.1$ MPa, $P_1 = 295.5$ MPa, and $\gamma = 7.44$ at 20 °C. When used in conjunction with the Gladstone–Dale relation, Eq. (6), ρ/ρ_0 cancels. Here, for the sake of comparison with other EoSs, we use the experimental value $\rho_0 = 998.2\ \mathrm{kg\,m^{-3}}$.

The phenomenological Tait equation is unphysical at negative pressures as it does not account for the existence of a limit of stability of the liquid, the spinodal pressure, at which the isothermal compressibility vanishes.[1] Instead, we use an equation that is based on physical grounds. The most recent international standard is the IAPWS-95,[25] which accounts for the existence of a liquid–vapor spinodal and predicts its pressure P_s to be around −160 MPa at 300 K. We have recently demonstrated the validity of extrapolating this equation down to −26 MPa at room temperature.[26] Figure 2 compares the above-mentioned EoS and a form developed by Speedy, which also accounts for the spinodal pressure P_s.[8] We provide the latter as an alternative to the IAPWS-95 as it is simpler to calculate while still providing a physical form,

$$P = P_s\left[1 - B\left(\frac{\rho}{\rho_s} - 1\right)^2\right], \tag{8}$$

with $P_s = -195.74$ MPa, $\rho_s = 818.26\ \mathrm{kg\,m^{-3}}$, and $B = 20.66$ at 20 °C. It agrees with the IAPWS-95 EoS within 0.7 MPa in the useful range of −50 to 200 MPa. In contrast, the difference between the Tait and IAPWS-95 EoSs is less than 0.7 MPa in a narrower range, between −50 and 30 MPa. Figure 2 also shows the increasing deviations between the EoSs with increasing negative pressure.

Strictly speaking, the liquid submitted to an acoustic wave follows an isentropic, and the applied pressure should be associated with a temperature change. For the IAPWS-95 and Speedy isotherms used above, we have neglected this change. This is justified by the small slope of the isentropic at ambient pressure,[3]

$$\left(\frac{\partial T}{\partial P}\right)_S = T\,V_{\mathrm{mol}}\,\frac{\alpha_P}{c_P}\,, \tag{9}$$

where V_{mol} and c_P are the molar volume and heat capacity at constant pressure, and α_P is the thermal expansion coefficient at constant pressure. Because α_P is zero in water at its density maximum close to 4 °C, the slope remains small in the range of interest. Using thermodynamic data, we have estimated a temperature change of less than 0.7 °C for cavitation at 50 °C.[3] A more accurate estimate can be made using the extrapolated EoS. For instance, the IAPWS-95 EoS gives an expression for the liquid entropy, from which a contour plot is easily generated (Fig. 3). It confirms that the temperature change can be neglected in the range of interest for acoustic cavitation experiments. In the following, we neglect the difference between the partial derivatives along an isentropic and an isotherm, omitting the usual corresponding subscripts.

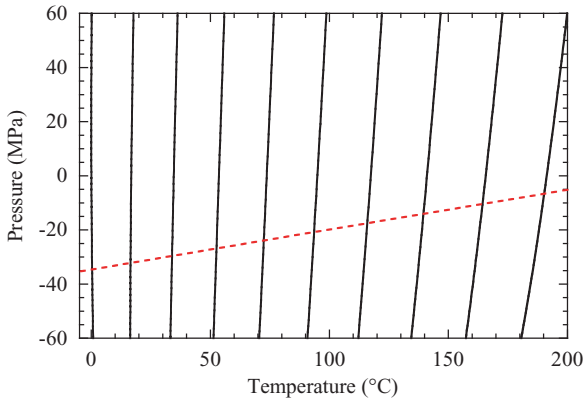

FIG. 3. (Color online) Isentropic lines for liquid water drawn in the pressure–temperature plane using the IAPWS-95 EoS. The entropy varies from 0 to 2250 $\mathrm{J\,kg^{-1}\,K^{-1}}$ in steps of 250 $\mathrm{J\,kg^{-1}\,K^{-1}}$ from left to right. The dashed red line shows schematically the lower limit of the pressure range investigated in acoustic cavitation experiments.

E. Correction for the compressibility of the fiber

Equation (5) directly gives $\delta n_l(t)$, the modulation of the refractive index of the liquid, if one assumes that the fiber index n_f remains constant. (We note that the index of fused silica has a very small temperature-dependance[27,28].) This is not the case since the fiber is submitted to stress by the sound wave. This was already emphasized in the original description of the FOPH.[7] However, for simplicity, n_f was considered "to be constant with regard to the compressibility of the fiber by a final pressure data correction of +3.6%, an approximation which holds for $n_f \simeq n_l$."[7] Indeed, in this case, Eq. (1) becomes

$$R \simeq \frac{1}{4}\left(1 - \frac{n_l}{n_f}\right)^2. \tag{10}$$

Let us use the superscripts c and nc for the values with and without correction for the compressibility of the fiber, respectively. Equation (10) yields

$$\frac{n_l^c - n_l^0}{n_l^{nc} - n_l^0} - 1 = \frac{\partial n_f/\partial P}{\partial n_l/\partial P} \equiv K\,. \tag{11}$$

To compute K, Ref. 7 takes

$$\frac{\partial n_f}{\partial P} \simeq 5 \times 10^{-6}\ \mathrm{MPa^{-1}} \text{ and } \frac{\partial n_l}{\partial P} \simeq 1.4 \times 10^{-4}\ \mathrm{MPa^{-1}}\,, \tag{12}$$

which leads to the +3.6% correction. Note that this correction is strictly on the index rather than on the pressure: they are slightly different because of the curvature of the EoS.

Here, we use a more refined approach and different values from Eq. (12). First, we do not limit the analysis to $n_f \simeq n_l$, but rather write the exact solution for n_l. For this, the change δn_f of the fiber index in the wave with respect to

its value at ambient pressure n_f is expressed as a function of the change δn_l of the liquid index $\delta n_f = K \delta n_l$. Equation (5) yields

$$\frac{\delta n_l}{n_l^0} = \frac{Q \frac{n_f^0}{n_l^0} - 1}{1 - KQ}, \tag{13}$$

where

$$Q = \frac{1 - \sqrt{R_0 + \delta R(t)}}{1 + \sqrt{R_0 + \delta R(t)}}. \tag{14}$$

Equation (13) shows that the correction increases with increasing Q, i.e., increasing n_l or ρ. In practice, in an experiment with water, Q always remains within a few percent of its value at ambient pressure, $Q_0 = n_l^0/n_f^0 \simeq 0.914$. If one wants to account for the compressibility of the fiber in a simpler way, the value obtained with n_f^0 can be multiplied directly by $1/(1 - KQ_0)$. To illustrate the difference with the treatment of Ref. 7, we first use the values displayed in Eq. (12) to compute K: this amounts to an index correction of $+3.4\%$ instead of the $+3.6\%$.

We have used the full formula [Eq. (13)] in our analysis. In addition, we have used a different value for K, writing

$$K = \frac{\partial \rho}{\partial n_l} \frac{\partial P}{\partial \rho} \frac{\partial n_f}{\partial P}. \tag{15}$$

$\partial \rho / \partial n_l$ is obtained by derivation of Eq. (A2), which gives 3124 kg m^{-3} at 20 °C. $\partial P / \partial \rho$ is the square of the sound velocity, 1482 m s^{-1} at 20 °C and 0.1 MPa.[25] These values give $\partial n_l / \partial P = 1.457 \times 10^{-4}$ MPa^{-1}. The quantity $\partial n_f / \partial P$ is less well known. The value 5×10^{-6} MPa^{-1} used in Ref. 7 is somewhat lower than one would expect. For instance, a simple estimate is obtained[29] by taking the derivative of the Lorentz–Lorenz relation and using the bulk modulus of silica $B_f = \rho_f (\partial P / \partial \rho_f)$,

$$\frac{\partial n_f}{\partial P} = \frac{(n_f^2 - 1)(n_f^2 + 2)}{6 n_f B_f}. \tag{16}$$

With $B_f = 37.02$ GPa (deduced from the sound velocity measurements of Ref. 30 using standard elasticity formulas), this gives 14.2×10^{-6} MPa^{-1}. In a direct compression experiment,[31] $\partial n_f / \partial \rho_f = 2.11 \times 10^{-4}$ m^3 kg^{-1} was obtained; $\rho_f = 2203$ kg m^{-3} and B_f yield $\partial n_f / \partial P = 12.6 \times 10^{-6}$ MPa^{-1}. Another, less accurate, value is found in a Brillouin scattering experiment on static compression of silica,[32] which used backscattering and plaquette geometries to obtain the sound velocity and the index of refraction independently. A quadratic fit to the $n_f(P)$ data is given, which yields $\partial n_f / \partial P = 11.5 \times 10^{-6}$ MPa^{-1}.

We have yet another way to estimate $\partial n_f / \partial P$ under the conditions of our experiment. It relies on the combination of the FOPH density data and the sound velocity measured in a time-resolved Brillouin scattering experiment at the acoustic focus.[26] These two measurements give access to the EoS of the liquid. The purpose is to measure the EoS in the metastable region, but the positive swing of the wave also gives data at positive pressure. $\partial n_f / \partial P$ can be treated as a fit parameter to optimize the agreement of our EoS measurement with accurate data at positive pressure. This procedure yields $\partial n_f / \partial P = (10.6 \pm 3) \times 10^{-6}$ MPa^{-1}. It is closer to the literature values than the value used in Ref. 7, but still slightly lower. This may be due to the different experimental conditions: the FOPH is subjected to a dynamic, inhomogeneous pressure field, rather than to pure hydrostatic compression. We have used $\partial n_f / \partial P = 10.6 \times 10^{-6}$ MPa^{-1} in all our analysis, including Ref. 13. With this value, the correction amounts to a relative increase in amplitude of around $+7.1\%$ in density and $+6.9\%$ in pressure, at 20 °C and near -30 MPa. For comparison, the inclusion of the stray light term, S, leads to a correction of $+1.4\%$ in pressure for the high directivity coupler used here. The effect of different choices for $\partial n_f / \partial P$ is shown in Sec. IV B.

F. Comparison with other measurements

We have compared the results from the FOPH to three other methods of measuring the amplitude of a sound wave. It is found to agree with measurements made using a commercial piezoelectric needle hydrophone (Precision Acoustics, UK) to within the large uncertainty due to the gain of the needle ($\pm 17\%$). It is also consistent with results using the "static pressure method"[3,13] and a two-dimensional interferometric measurement.[33] The former is an indirect estimate of the pressure and the latter requires more sophisticated optical alignment, neither of which are suitable for the current study.

IV. APPLICATION TO ACOUSTIC CAVITATION IN WATER

The transformation of a liquid into a vapor is a first order transition. At each temperature, the two phases coexist in stable equilibrium at the saturated vapor pressure $P_{sat}(T)$. But the liquid phase can be prepared at a reduced pressure $P < P_{sat}(T)$, for instance, during the rarefaction swing of an acoustic wave. The liquid is then metastable compared to the vapor and has a finite lifetime because an energy barrier E_b has to be overcome for the vapor phase to appear.[1] We have studied the limiting pressure to which the liquid can be brought in an acoustic wave before nucleation of vapor occurs.[3,13] Up to now we have reported results obtained with bursts of a 1 MHz ultrasonic wave [and preliminary data at 1.3 MHz (Ref. 34)]. It is interesting to check the effect of changing the frequency of the wave because this changes both the duration and volume of the applied stress. Here we report new results using a 2 MHz acoustic wave and their interpretation in light of nucleation theory.

A. Experimental procedure

The setup used to generate acoustic waves is described in Sec. II A. Full details on the cavitation measurement can be found in our earlier publications.[3,13] In brief, when acoustic bursts of sufficient amplitude are repeated under the same

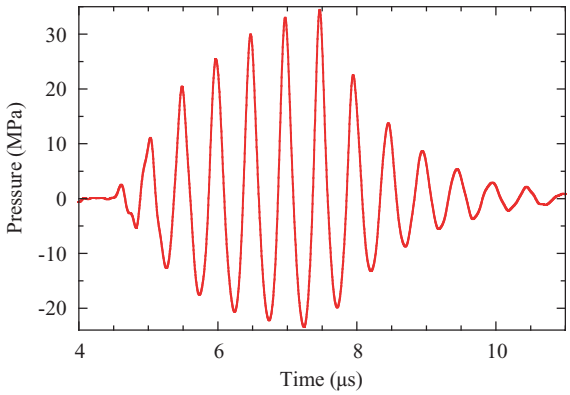

FIG. 4. (Color online) Pressure waveform measured by the FOPH at the acoustic focus of a 2 MHz transducer, driven by a six-cycle burst starting at the time origin, at an amplitude of 0.627 V_{cav} and at a temperature of 10.5 °C.

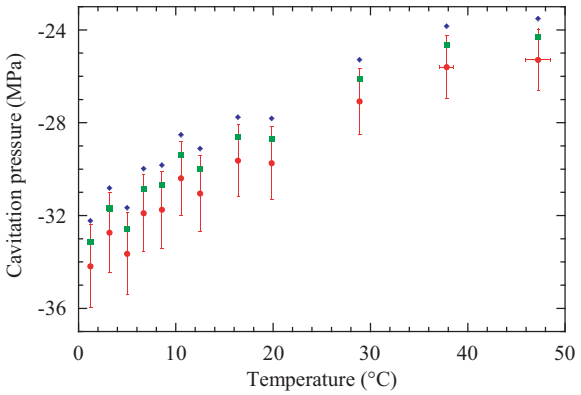

FIG. 5. (Color online) Cavitation pressure at 1 MHz as a function of temperature. Three values of $\partial n_f/\partial P$ have been used to correct for the compressibility of the fiber: 0 (blue diamonds), 5 (green squares), and 10.6×10^{-6} MPa^{-1} (red circles). For clarity, the error bars are shown for the red circles only.

experimental conditions, we observe random cavitation events. Their probability Σ is measured over a large number of bursts (typically 400), as a function of the rms voltage V_{rms} of the driving burst. The result is well described by a double exponential function,[3]

$$\Sigma(V_{rms}) = 1 - \exp\left\{-\ln 2 \exp\left[\xi\left(\frac{V_{rms}}{V_{cav}} - 1\right)\right]\right\}, \qquad (17)$$

which we call an S-curve owing to its shape. The cavitation voltage V_{cav} is the value of V_{rms} for which $\Sigma = 1/2$, and ξ is the steepness of the S-curve. Before and after each experiment, an S-curve is measured.

Detailed maps of the acoustic field amplitude corroborate an ellipsoidal shape of the focus ($\lambda \times \lambda \times 2\lambda$, $\lambda \approx 1.5$ mm at 1 MHz). Their quality is such that secondary and weak tertiary maxima can be identified. This shows that the size of the fiber (core/clad of 50/125 μm) does not disturb the acoustic field. In order to measure $P_{cav}(T)$, we performed experiments at temperatures between 0 and 50 °C. A map is taken at each temperature in order to locate the acoustic focus, although no measurable shift in the position of the focus was found, and then the excitation voltage is ramped from 0.1 to 0.6V_{cav}.

Figure 4 shows a typical $P(t)$ waveform for a 2 MHz acoustic burst. In order to obtain P_{cav}, we measure the minimum of $P(t)$ as a function of V_{rms}, stopping at 0.6 V_{cav} to avoid cavitation damage on the fiber tip. We then extrapolate with a parabola up to V_{cav}. We have checked at 20 °C and at the extrema of the temperature range that this extrapolation correctly reproduces the data up to 0.9 V_{cav}.[13] Repeated checks of the data at a reference temperature were performed to ensure that no damage occurred, otherwise the fiber was recleaved.

To determine the statistical error of our setup, a series of 26 measurements were taken at 20 °C. Their scatter includes all possible random effects and gives a standard deviation of 5.4%, which was used for all temperatures.

B. Cavitation pressure

The pressure at the cavitation threshold (P_{cav}) determined from extrapolations of the parabolic fit are shown in Fig. 5. Three sets of data are displayed: one assumes n_f to be constant; the second uses values of Ref. 7 to compute K in Eq. (13); the third uses our preferred value for $K = 10.6 \times 10^{-6}$ MPa^{-1}. It can be seen that the differences between the successive data sets are of the order of the error bars, but as a systematic effect, it should not be ignored.

We have explained elsewhere[2,3] that although our results on acoustic cavitation are highly reproducible and close to those obtained with other methods, they are far from the theoretical prediction for homogeneous nucleation, which is approached by only one experiment using microscopic inclusions of water in quartz. For a discussion of this discrepancy, we refer the reader to Ref. 13. Here, we focus on the frequency dependence of acoustic cavitation and use it as a test of nucleation theory.

C. Frequency dependence of the cavitation threshold

Nucleation theory assumes that the nucleation rate follows an Arrhenius law,

$$\Gamma = \Gamma_0 \exp\left(-\frac{E_b(P)}{k_b T}\right), \qquad (18)$$

where Γ_0 is a prefactor. Several choices for Γ_0 are possible;[1,35] however, this quantity cancels out in the following analysis since it depends only weakly on frequency. A nucleation probability of 50% is reached at the cavitation pressure P_{cav} that satisfies

$$\Gamma_0 V_{exp} \tau_{exp} \exp\left(-\frac{E_b(P_{cav})}{k_b T}\right) = \ln 2, \qquad (19)$$

for an experiment in which a negative pressure is applied to a volume V_{exp} of liquid during a time τ_{exp}. As the time and length scales in an acoustic wave are determined by its period τ, $V_{exp}\tau_{exp} \propto \tau^4$ (see Appendix B for the exact expression). When changing the frequency $f = 1/\tau$ from f_1 to f_2, nucleation theory thus predicts the associated change in E_b to be,

$$\frac{E_{b,2} - E_{b,1}}{k_b T} = 4 \ln \frac{f_1}{f_2}. \qquad (20)$$

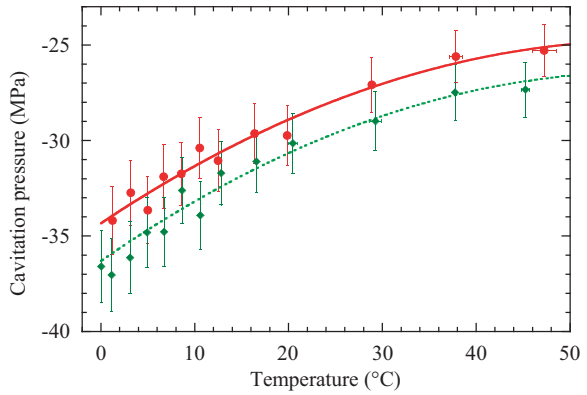

FIG. 6. (Color online) Cavitation pressure as a function of temperature. Red circles and green diamonds show the data obtained with the FOPH at 1 and 2 MHz, respectively. The solid red curve is a parabolic fit to the 1 MHz data and gives the dotted green curve when multiplied by the amount predicted by Eq. (22).

Furthermore, from the steepness ξ of the S-curve, we know [Eq. (13) of Ref. 3]

$$\left(\frac{\partial E_b}{\partial P}\right)(P_{cav}) = -\frac{k_b T}{P_{cav}}\xi\,. \tag{21}$$

Because of the high stability required to obtain sufficient statistics, the data for ξ were obtained in a high pressure cell.[3,13] A linear fit gives $\xi = 45.9 - 0.120\,T$ with T in degrees Celsius between 0 and 60 °C.

From Eqs. (20) and (21) and linearizing $E_b(P)$, we can predict the change in P_{cav},

$$\frac{P_{cav,2}}{P_{cav,1}} = 1 + \frac{4}{\xi}\ln\frac{f_2}{f_1}\,, \tag{22}$$

and compare it with the experiment. This is shown in Fig. 6, where FOPH measurements at $f_1 = 1.03$ MHz and $f_2 = 1.99$ MHz are shown. A parabolic fit to the results at f_1 gives $P_{cav} = -34.3 + 0.327\,T - 0.00280\,T^2$ with P_{cav} in megapascals and T in degrees Celsius. Multiplying by the amount given in Eq. (22) yields a prediction at f_2, which passes through the data. Even if the statistical error bars are comparable to the predicted change in P_{cav}, the systematic difference between the data at two frequencies is well reproduced using only experimentally determined quantities and without any additional fitting parameter. We emphasize that the above reasoning is based upon general arguments about nucleation theory and not on the details of the microscopic model for nucleation. This explains why we chose a parabolic fit to $P_{cav}(T)$, instead of an analysis based on a specific nucleation model as in Ref. 13.

V. CONCLUSION

The fiber optic probe hydrophone is a valuable tool for nucleation studies because it gives an absolute pressure measurement close to the cavitation threshold. We have built a FOPH as proposed in Ref. 7, improving on the calibration method, and using physically justifiable relations to convert the measured refractive index to the liquid density and subsequently to the pressure. This is of particular importance when measuring negative pressures. Overall, the approximations made in the original work are warranted. The most consequential change we propose is in the correction made to account for the compressibility of the optical fiber. The correction is not a uniform change, and more importantly, at the acoustic cavitation threshold in water, it is two times larger than originally proposed.

We have used the FOPH to investigate the dependence of the nucleation threshold on the size and duration of the experiment. The results are in good agreement with general nucleation theory, which is independent of any detailed model for the nucleation mechanism.

ACKNOWLEDGMENTS

We thank S. Cersoy, J. Dubail, and R. Sheshka for their participation in early stages of the experiment. This research has been funded by the ERC under the European Community's FP7 Grant Agreement No. 240113.

APPENDIX A: RELATION BETWEEN INDEX AND DENSITY

Here we provide details about the relation between n_l and ρ discussed in Sec. III C. We have used the IAPWS formulation,[23] which is based on a modified version of the Lorentz–Lorenz [24] relation,

$$\frac{n_l^2-1}{n_l^2+2}\frac{1}{\bar\rho} = a_0 + a_1\bar\rho + a_2\bar T + a_3\bar\lambda^2\bar T + \frac{a_4}{\bar\lambda^2} + \frac{a_5}{\bar\lambda^2 - \bar\lambda_{UV}^{\,2}} + \frac{a_6}{\bar\lambda^2 - \bar\lambda_{IR}^{\,2}} + a_7\bar\rho^2, \tag{A1}$$

where $\bar\rho = \rho/\rho^*$ with $\rho^* = 1000\ \mathrm{kg\,m^{-3}}$, $\bar T = T/T^*$ with $T^* = 273.15$ K, and $\bar\lambda = \lambda/\lambda^*$ with $\lambda^* = 589$ nm. The other parameters can be found in Ref. 23. For our purpose, since $\lambda = 808$ nm, Eq. (A1) reduces to

$$\frac{n_l^2-1}{n_l^2+2} = \bar\rho\left[b(\bar T) + a_1\bar\rho + a_7\bar\rho^2\right], \tag{A2}$$

with $b(\bar T) = 0.213854 - 3.22673\times10^{-3}\,\bar T$, $a_1 = 9.74634476\times10^{-3}$, and $a_7 = -1.66626219\times10^{-2}$. Equation (A2) is a cubic equation in $\bar\rho$, whose discriminant is positive for typical values of T and n_l. It has therefore three solutions: numerical inspection shows that one is negative and two are positive, and the one of interest lies close to 1.

APPENDIX B: DETERMINATION OF THE EXPERIMENTAL VOLUME AND TIME IN AN ACOUSTIC CAVITATION EXPERIMENT

Here we justify the form $V_{exp}\tau_{exp} \propto \tau^4$ taken to analyze the frequency dependence of the cavitation threshold (Sec. IV C). Let us first recall the approach used in Ref. 35 to analyze acoustic cavitation data obtained in liquid helium 4. In an acoustic cavitation experiment, the pressure varies in space and time. Setting the origin of time and space where the pressure reaches its minimum P_{min}, the wave of wavenumber

$k = (2\pi)/\lambda$ and period τ can be approximated by

$$P(\mathbf{r}, t) = P_{\min} \frac{\sin(kr)}{kr} \cos\left(2\pi \frac{t}{\tau}\right) \simeq P_{\min}(1-ar^2)(1-bt^2) \tag{B1}$$

near the minimum, with

$$a = \frac{2\pi^2}{3\lambda^2} \quad \text{and} \quad b = \frac{2\pi^2}{\tau^2}. \tag{B2}$$

The local nucleation rate per unit volume and time writes

$$\Gamma(\mathbf{r}, t) = \Gamma_0 \exp\left(-\frac{E_b\,[P(\mathbf{r}, t)]}{k_b T}\right). \tag{B3}$$

The quantity measured in the experiment is the probability Σ that cavitation occurs for acoustic bursts repeated under the same conditions, namely, the liquid temperature and the minimum pressure reached in the wave $P_{\min}$. For the stochastic process with a rate $\Gamma(\mathbf{r}, t)$, integrating over space and time gives

$$\begin{aligned}\Sigma &= 1 - \exp\left[\int \mathrm{d}\mathbf{r}\mathrm{d}t\, \Gamma(\mathbf{r}, t)\right] \\ &= 1 - \exp\left[-\frac{\pi^2 \Gamma_0}{a^{3/2} b^{1/2}} \left(\frac{k_b T}{P_{\min}(\partial E/\partial P)}\right)^2 \right. \\ &\qquad \left. \times \exp\left(-\frac{E_b(P_{\min})}{k_b T}\right)\right].\end{aligned} \tag{B4}$$

The system behaves as if the pressure $P_{\min}$ was held constant over an experimental volume $V_{\exp}$ and during an experimental time $\tau_{\exp}$ such that

$$V_{\exp}\tau_{\exp} = \frac{3^{3/2}\lambda^3 \tau}{4\pi^2} \left(\frac{k_b T}{P_{\min}(\partial E/\partial P)}\right)^2. \tag{B5}$$

From the nucleation theorem,[36] we have the volume of the critical bubble for nucleation, $V_c = (\partial E/\partial P)_T$.[13] This is known experimentally from the steepness ξ of the S-curves [Eq. (21)]. Finally, Eq. (19) can be rewritten as

$$\frac{3^{3/2}}{4\pi^2} \frac{k_b T}{h} \frac{c^3}{V_c \xi^2 f^4} \exp\left(-\frac{E_b(P_{\text{cav}})}{k_b T}\right) = \ln 2, \tag{B6}$$

where we have introduced the sound velocity c and the frequency f of the wave. Strictly speaking, Eq. (20) is thus

$$\frac{E_{b,2} - E_{b,1}}{k_b T} = 4 \ln \frac{f_1}{f_2} + \ln \frac{(V_c \xi^2)_1}{(V_c \xi^2)_2}. \tag{B7}$$

Between 1 and 2 MHz, P_{cav} varies only by 7% (see Fig. 6). Over this reduced interval, the quantity $V_c \xi^2$ shows only small variations, which can be neglected compared to the factor 16 change in f^4.

[1] P. G. Debenedetti, *Metastable Liquids* (Princeton University Press, Princeton, NJ, 1996).
[2] F. Caupin and E. Herbert, C. R. Phys. **7**, 1000 (2006).
[3] E. Herbert, S. Balibar, and F. Caupin, Phys. Rev. E **74**, 041603 (2006).
[4] B. Zeqiri, Prog. Biophys. Mol. Biol. **93**, 138 (2007).
[5] R. O. Cleveland, M. R. Bailey, N. Fineberg, B. Hartenbaum, M. Lokhandwalla, J. A. McAteer, and B. Sturtevant, Rev. Sci. Instrum. **71**, 2514 (2000).
[6] A. Shaw and M. Hodnett, Ultrasonics **48**, 234 (2008).
[7] J. Staudenraus and W. Eisenmenger, Ultrasonics **31**, 267 (1993).
[8] R. J. Speedy, J. Phys. Chem. **86**, 982 (1982).
[9] P. H. Poole, F. Sciortino, U. Essmann, and H. E. Stanley, Nature (London) **360**, 324 (1992).
[10] S. Sastry, P. G. Debenedetti, F. Sciortino, and H. E. Stanley, Phys. Rev. E **53**, 6144 (1996).
[11] F. Caupin, Phys. Rev. E **71**, 051605 (2005).
[12] Q. Zheng, D. J. Durben, G. H. Wolf, and C. A. Angell, Science **254**, 829 (1991).
[13] K. Davitt, A. Arvengas, and F. Caupin, EPL **90**, 16002 (2010).
[14] Éric Herbert, Ph.D. dissertation, Université Paris-Diderot, Paris VII, 2006
[15] J. E. Parsons, C. A. Cain, and J. B. Fowlkes, J. Acoust. Soc. Am. **119**, 1432 (2006).
[16] P. C. Beard and T. N. Mills, Appl. Opt. **35**, 663 (1996).
[17] C. Koch, Ultrasonics **34**, 687 (1996).
[18] Y. Uno and K. Nakamura, Jpn. J. Appl. Phys. **38**, 3120 (1999).
[19] P. Lewin, C. Mu, S. Umchid, A. Daryoush, and M. El-Sherif, Ultrasonics **43**, 815 (2005).
[20] R. G. Minasamudram, P. Arora, G. Gandhi, A. S. Daryoush, M. A. El-Sherif, and P. A. Lewin, Appl. Opt., **48**, G77 (2009).
[21] R. Pecha, "*FOPH 2000: Technical Description and Instruction Manual*" (RP Acoustics, Leutenbach, Germany, 1996).
[22] I. H. Malitson, J. Opt. Soc. Am. **55**, 1205 (1965).
[23] The International Association for the Properties of Water and Steam, *Release on the Refractive Index of Ordinary Water Substance as a Function of Wavelength, Temperature and Pressure* (IAPWS, Germany, 1997). See http://www.iapws.org/relguide/rindex.pdf.
[24] M. Born and E. Wolf, *Principles of Optics* (Cambridge University Press, Cambridge, UK, 1999).
[25] The International Association for the Properties of Water and Steam, *Revised Release on the IAPWS Formulation 1995 for the Thermodynamic Properties of Ordinary Water Substance For General and Scientific Use* (IAPWS, Germany, 2009). See http://www.iapws.org/relguide/IAPWS95-Rev.pdf.
[26] K. Davitt, E. Rolley, F. Caupin, A. Arvengas, and S. Balibar, J. Chem. Phys. **133**, 174507 (2010).
[27] T. Toyoda and M. Yabe, J. Phys. D: Appl. Phys. **16**, L97 (1983).
[28] D. B. Leviton and B. J. Frey, in *Optomechanical Technologies for Astronomy* edited by E. Atad-Ettedgui, J. Antebi, and D. Lemke (SPIE, Orlando, FL, USA, 2006), Vol. **6273**, pp. 62732K–11
[29] F. Pockels, Ann. Phys. **312**, 745 (1902).
[30] H. J. McSkimin, J. Acoust. Soc. Am. **31**, 287 (1959).
[31] R. G. Kuryaeva and V. A. Kirkinskii, Phys. Chem. Miner. **25**, 48 (1997).
[32] C. S. Zha, R. J. Hemley, H. K. Mao, T. S. Duffy, and C. Meade, Phys. Rev. B **50**, 13105 (1994).
[33] F. Souris, J. Grucker, J. Dupont-Roc, P. Jacquier, A. Arvengas, and F. Caupin, Appl. Opt. **49**, 6127 (2010).
[34] E. Herbert and F. Caupin, J. Phys. Condens. Matter **17**, S3597 (2005).
[35] M. S. Pettersen, S. Balibar, and H. J. Maris, Phys. Rev. B **49**, 12062 (1994).
[36] D. W. Oxtoby and D. Kashchiev, J. Chem. Phys. **100**, 7665 (1994).